Title

Reshaping the Endogenous Electric Field to Boost Wound Repair via Electrogenerative Dressing

Ruizeng Luo, Yi Liang, Jinrui Yang, Hongqing Feng, Ying Chen, Xupin Jiang, Ze Zhang, Jie Liu, Yuan Bai, Jiangtao Xue, Shengyu Chao, Yi Xi, Xiaoqiang Liu, Engui Wang, Dan Luo, Zhou Li*, Jiaping Zhang**

R. Luo, Y. Liang, J. Yang, Y. Chen, X. Jiang, Z. Zhang, J. Liu, X. Liu, J. Zhang

Department of Plastic Surgery, State Key Laboratory of Trauma, Burns and Combined Injury, Southwest Hospital, Third Military Medical University (Army Medical University); Chongqing, 400038, China.

Email: japzhang@aliyun.com

R. Luo, H. Feng, Y. Bai, T. Xue, S. Chao, E. Wang, D. Luo, Z. Li

Beijing Institute of Nanoenergy and Nanosystems, Chinese Academy of Sciences; Beijing, 101400, China.

Email: luodan@binn.cas.cn (Dan Luo), zli@binn.cas.cn (Zhou Li)

R. Luo, H. Feng, S. Chao, D. Luo, Z. Li

School of Nanoscience and Technology, University of Chinese Academy of Sciences; Beijing, 100049, China.

Y. Liang

Department of Burn and Plastic Surgery, Army 73rd Group Military Hospital; Xiamen, 361000, China.

Y. Bai, D. Luo, Z. Li

Center on Nanoenergy Research, School of Physical Science & Technology, Guangxi University; Nanning, 530004, China.

T. Xue

This article has been accepted for publication and undergone full peer review but has not been through the copyediting, typesetting, pagination and proofreading process, which may lead to differences between this version and the Version of Record. Please cite this article as doi: 10.1002/adma.202208395.

Institute of Engineering Medicine, Beijing Institute of Technology; Beijing, 100081, China.

Y. Xi

Chongqing Key Laboratory of Soft Condensed Matter Physics and Smart Materials, Department of Applied Physics, State Key Laboratory of Power Transmission Equipment & System Security and New Technology, Chongqing University, Chongqing 400044, P. R. China.

Z. Li

Institute for Stem Cell and Regeneration, Chinese Academy of Sciences, Beijing 100101, China.

Keywords: self-powered electrical simulation dressing, epithelial regeneration, triboelectric nanogenerator, electric field therapy, negative pressure wound therapy

Abstract

The endogenous electric field (EF) generated by transepithelial potential difference plays a decisive role in wound re-epithelialization. For patients with large or chronic wounds, negative pressure wound therapy (NPWT) is the most effective clinical method in inflammation control by continuously removing the necrotic tissues or infected substances, thus creating a pro-proliferative microenvironment beneficial for wound re-epithelialization. However, continuous negative pressure drainage causes electrolyte loss and weakens the endogenous EF, which in turn hinders wound re-epithelialization. Here, we developed an electrogenerative dressing (EGD) by integrating triboelectric nanogenerators with NPWT. By converting the negative pressure-induced mechanical deformation into electricity, EGD produced a stable and high-safety EF that could trigger a robust epithelial electrotactic response and drive the macrophages toward a reparative M2 phenotype *in vitro*. Translational medicine studies confirmed that EGD completely reshaped the wound EF weakened by NPWT, and promoted wound closure by facilitating an earlier transition of inflammation/proliferation and guiding epithelial migration and proliferation to accelerate re-epithelialization. Long-term EGD therapy remarkably advanced tissue remodeling with mature epithelium, orderly extracellular matrix and less scar formation. Compared with the golden standard of NPWT, EGD orchestrated all the essential wound stages in a non-invasive manner, presenting an excellent prospect in clinical wound therapy.

1. Introduction

The skin, which is composed of epidermis and dermis, is the first barrier of the human body. Damage to the barrier function generates an unsealed wound, preventing protection against further environmental damage or pathogens, causing health issues in patients [1]. The repair of skin wounds is a complex multi-step process involving overlapping stages of hemostasis, inflammation, proliferation, and remodeling [2]. Among these stages, the proliferative stage, as characterized by the formation of granulation tissue and re-epithelialization, is crucial for wound repair. Nevertheless, accumulating evidence indicates that a transition from the inflammatory to the proliferative stage is a key step during the healing progress, which is usually correlated to the transformation of macrophages from a pro-inflammatory M1 to a reparative M2 phenotype. Prolonged inflammation or failed macrophages M2 transition impedes the progress into the proliferative phase, and ultimately results in impaired healing, e.g., chronic wound or excessive scarring, which presents a major and increasing health and economic burden to our society [3]. To date, wound dressing is still the main clinical care modality, and many dressing care strategies have been established for different types of wounds [4]. In recent decades, negative pressure wound treatment (NPWT) has become the gold standard in controlling inflammation in large or chronic wounds [5]. As a widely accepted technique, NPWT initially seals the wound with a dressing and then drains wound exudates through negative pressure, thereby reducing the risk of infection, protecting the wound microenvironment, and ultimately, promoting the growth of granulation tissue [5]. Although NPWT is beneficial for inflammation control, clinical evidence shows that it has a poor direct effect on wound re-epithelialization, a well-known most important feature of a healed wound [6]. This dilemma emphasizes the importance of an in-depth understanding of the NPWT mechanism, and the development of new combined strategies to actively activate wound re-epithelialization while facilitating inflammation/proliferation transition, thereby accelerating wound repair and reducing scarring.

The fact that NPWT can eliminate exudates and cause electrolyte loss has been widely recognized by clinicians. This clue is suspected to be related to the difficulty of re-epithelialization. Since Emil Du-Bois Reymond first recorded the wound current more than hundred years ago, subsequent studies confirmed that the endogenous EF exists in various animals, and plays an essential role in wound re-epithelialization by guiding the migration of the electroactive key cells, such as epithelial cells [7]. The transepithelial potential of the normal epidermis is the basis of wound endogenous EF. Due to the asymmetric distribution of ion channels in epithelial cells, cations (Na^+) are transported to the epidermal basal side and anions (Cl^-) are transported to the epidermal apical side, creating transepithelial potential. When a wound occurs, a current is driven out of the injury, and the flow of

the current creates a lateral EF with the edge of the wound as the anode and the center as the cathode [8, 9]. Based on the above understanding, it is reasonable to speculate that the loss of electrolytes in the wound under NPWT might attenuate the wound current and ultimately weaken the endogenous EF. More importantly, the theory that weakening the endogenous EF causes hard-to-heal wounds has been verified in some metabolic disease models, such as diabetes [10].

Based on the above-mentioned theory, electrical therapy might effectively complement NPWT, and achieve synergistic wound healing by reshaping the EF. Although there has been some evidence that DC power can guide the directional migration of epithelial cells [9, 11, 12], its poor portability, high operational risk, and unclear mechanisms limit an in-depth study. Urgent demand requires a safe, convenient, integrated, and self-powered electricity supply system to be integrated with NPWT, achieving long-term, uninterrupted treatment. The triboelectric nanogenerator (TENG) is a novel energy supply system, proposed by Prof. Zhong-Lin Wang in 2012; it can collect tiny amounts of mechanical energy and convert it into periodic electrical pulses [13]. Benefiting from its characteristics of controllable parameters, portable design, flexible operation, and a high degree of safety [14], the vertical-contact separation mode of TENGs has been widely used to drive a variety of self-powered biosensors and pacemakers [15, 16]. Self-powered electrical stimulation devices based on TENGs undoubtedly provide a feasible solution for wound treatment.

In light of these considerations, we here designed an electrogenerative dressing (EGD) based on the combination of NPWT and TENGs, aimed at the issue of the increasing clinical need for large or chronic full-thickness skin wound treatment. In a closed environment, the NPWT controlled the pressure change in the dressing regularly, driving the integrated TENG to convert the mechanical energy generated by the shrinkage and relaxation of the dressing into electricity, forming a compensating EF to stimulate wound repair. *In vitro* evidence showed that the EGD-generated EF triggered a robust epithelial electrotactic response, and drove macrophages toward a reparative M2 phenotype, without any adverse effect on cells due to its extremely low current. The subsequent large animal experiments showed that the EDG, reshaping the wound EF weakened by NPWT completely, expedited the proliferation period by promoting the transition of inflammation/proliferation, and accelerated wound re-epithelialization by guiding migration and proliferation of epithelial cells. Moreover, EGD also advanced the remodeling period by rebuilding a mature epithelial microstructure and orderly extracellular matrix, thereby improving repair quality and reducing scar formation. In brief, the self-powered EF generated by EGD acted as an “electric adjuvant” that perfectly orchestrated almost all the essential stages of wound repair in a non-invasive manner, thus revealing its extensive clinical prospects.

2. Results and discussion

Materials, designs, integration structure and performance characteristics of the EGD

A typical EGD system consists of two core components: NPWT (negative pressure control device (NCD) and foam dressing) and a self-powered electrical simulation system (TENG, rectifier, and electrodes) **(Figure 1A-1C and Figure. S1, Supporting Information)**. The polyurethane foam dressing, possessing a porous structure with an average pore size of 260 μm, was connected with the NCD to form an integral NPWT system **(Figure 1A)**. The porous structure ensured that negative pressure was transmitted to the wound surface and drove the dressing to be compressed and relaxed periodically, under the rhythmic work of the inflator and sucking pumps. According to the deformation characteristics of the dressing, the TENG in vertical contact-separation mode was selected and integrated into the upper layer of the dressing **(Figure 1B)**. The TENG consisted of two friction layers (Al and PTFE), two support substrates (PET), two electrode layers (Cu and Al), a spacer layer, and an encapsulation layer (Kapton). The polished friction layers formed a strip-like surface microstructure, which increased the contact area and ultimately improved the output of the TENG. The presence of support substrates facilitated the separation of the TENG friction layer; and the encapsulation layer prevented the TENG from being eroded by exudates, thereby improving the stability of the TENG. The periodic deformation of the dressing drove the contact-separation of the TENG friction layers, which drove the electron flow and generated an electric potential. The naturally formed endogenous EF in the wound tends to have a fixed direction and, in contrast to the wound edge, the wound center acts as a cathode. To simulate the directionality of the endogenous EF, a rectifier was integrated into the dressing to change the output direction of the built-in TENG. In addition, electrodes that can produce an oriented EF were connected to the bottom of the dressing; the annular electrode was placed around the wound edge as the anode, and the center electrode was placed on the wound center as the cathode **(Figure 1A and 1C)**.

The electricity generation principle of the EGD is attributed to the difference in electron affinity between PTFE with Al in the TENG **(Figure. 1D and Figure. S2, Supporting Information)**. When the vacuum pump operated, the internal negative pressure gradually increased, the dressing was compressed and the friction layers of the internal TENG came into contact, generating opposite charges on the surface [17]. As the air pump operated, the negative pressure was gradually neutralized, and the two friction layers were then separated. The regular change of negative pressure drove the periodic relative displacement of the PTFE and Al layer, accompanied by the electrons

flowing back and forth between the two electrodes, thereby generating alternating current in the external circuit. The corresponding relationship between the output performance of the TENG and NPWT was systematically studied. By adjusting the inflating and exhaust time, eight clinically commonly used NPWT parameters were selected, and the internal pressure, peak value of open-circuit voltage and short-circuit current of the EGD in each mode were further monitored to screen out preliminarily the best working condition **(Figure 1E-1H and Figure S3, Supporting Information)**. The 5^{th} -8^{th} NPWT modes were initially eliminated, because EGD generated positive pressure in these modes, which was adverse on controlling inflammation and maintaining the stability of electric field therapy. The 1^{st} -4^{th} modes could effectively implement NPWT, and the open-circuit voltage and short-circuit current of the EGD were positively correlated with the change of internal negative pressure, which was caused by an increase in the relative contact area between the built-in TENG friction layers under high negative pressure [18]. Taking into account the clinical therapeutic window of NPWT (optimum negative pressure interval: -75 ~ -150 mmHg) [6], the 4^{th} NPWT mode (pump-down for 3s, inflation for 1s) was chosen as the best working condition; the peak value of the open-circuit voltage was 4.7 V and the short-circuit current was 100 nA **(Figure S3, Supporting Information)**. The maximum voltage after full-wave rectification was ~ 4 V, and the current was ~ 28 nA **(Figure 1E and 1F)**. The TENG can provide robust and continuous electrical output; after a treatment cycle (6 days), the EGD still maintained 92%~93% of the initial open circuit voltage (**Figure S4, Supporting Information**).

EGD reshaped the wound EF weakened by NPWT

Drainage of exudate from the wound is the basic treatment principle of NPWT [19]. The accompanying loss of electrolytes (Na^+, Cl^-, K^+, etc.) in local tissues may affect the wound current, thereby weakening the endogenous EF **(Figure 2A and Figure S5, Supporting Information)**. The Bama pig model showed the volcanic distribution of the EF in a normal wound had a potential difference of ~70 mV **(Figure 2A, 2D)**. As the negative pressure drainage started, the potential difference gradually decreased to ~40 mV within 3 hours **(Figure 2B, 2D)**. With prolonged NPWT, the damaged tissue continued to maintain a low potential level, only ~65% of the initial value **(Figure 2E)**, which is comparable to the decreasing trend of wound potential in the diabetic wound [10]. Interestingly, the decrease in EF by NPWT can be completely reversed by EGD therapy **(Figure 2C)**. EGD converted the mechanical energy generated by the rhythmic deformation of the dressing into electrical output. The potential generated by the built-in TENG was rectified and applied to the wound through electrodes, enhancing the potential difference between wound edge and wound center attenuated by NPWT,

thereby reshaping the wound's EF. The average wound's EF intensity in the EGD group was 197 mV/mm, which was 3.5 and 5.2 times that of the Blank and NPWT group, respectively **(Figure 2A-2C)**. As a natural capacitor, the skin can be quickly charged by TENG. When the TENG was turned on, the potential of the wound climbed from ~40 mV to ~250 mV and reached saturation within 0.5 hours. However, the electric potential quickly fell back to the level of NPWT, as the TENG was turned off **(Figure 2F)**. Moreover, the amplified curve showed that the pulse signal could be extracted from the wound current of the EGD group, the frequency of which was consistent with that of the rectified TENG **(Figure 2G, Figure 1F)**, revealing that the reshaped EF was mainly due to the contribution of the TENG.

Biosafety assessment of EGD treatment

Many concerns about the biological safety of electrotherapy have mainly focused on the thermal injury caused by the electric current. Commercial electrical stimulators driven by an external DC power source often have very high currents, which can easily cause obvious cell damage [20]. In contrast, the pulse current output by the TENG after rectification is much smaller, ensuring safety during treatment **(Figure 3A)**. To show quantitatively the safety gap between DC, PC, and TENG, the theoretical thermal energies generated by the two treatment methods were calculated. The output current of the built-in TENG in the EGD could be calculated by the following formula:

$$I(t) = isin(\omega t + \varphi) \qquad \text{(Equation 1)}$$

where *I* is the current amplitude, *t* is the duration, ***i*** is the intensity of the current, and ω and φ are the period and the initial phase of the sine function, respectively. The thermal energy is determined as follows:

$$dW_h = \eta R I^2(t) dt \qquad \text{(Equation 2)}$$

where dW_h is the thermal energy produced by the current ***i*** in the time ***t***, dw is the electrical work of the current, the resistance of the load is R, and η is the thermal efficiency of the current. Based on the above formula, the relationship between current thermal energy (W_h) and surface integral (*i*) can be established as follows:

$$W_h = \eta R \int_0^{t_0} i^2 sin^2(\omega t + \varphi)\, dt \quad \text{(Equation 3)}$$

According to this calculation, we confirmed that the thermal energy of the EGD was one-trillionth that of the DC and the 10 millionths of PC **(Figure 3B, Figure S6, Supporting Information)**. Cell viability under different electrical stimulation conditions was quantified using a CCK-8 test. After comparing with the Blank group, TENG had no adverse effect on human immortalized keratinocytes (HaCaT) within 48 h, and its cytocompatibility was significantly better than that of the DC and PC

group **(Figure 3C)**. Live/dead staining images also showed consistent results, wherein more cells in the DC and PC groups were dead due to the accumulation of heat energy **(Figure 3D)**.

EGD-generated EF empowered HaCaT cells with robust electrotactic response *in vitro*

To determine whether the pulsed electric output by EGD could effectively drive the electrotaxis of epithelial cells **(Figure 3E)**, a migration experiment was carried out by seeding HaCaT cells on a conductive medium and an exogenous EF generated by the EGD when using the 4th NPWT parameter (pumped for 3s and inflated for 1s) was applied to the endowed cells **(Figure S7, Supporting Information)**. The optical microscope images showed that the cell migration in the Blank group (free migration without an EF) within 3 hours was neither significant nor directional. In contrast, the EF generated by the EGD promoted the migration of the HaCaT cells and induced their directional movement significantly **(Figure 3F, Figure S8 and Video S1, Supporting Information)**. The cell trajectories of the two groups were summarized in a 2D chart **(Figure 3G)**, and the displacement speed, trajectory speed, and directionality cos θ of the HaCaT cells were further calculated **(Figure 3H)**. Notably, the displacement speed in the EGD group was 6 times that of the Blank group, and the directedness in the EGD group ($|\cos(\theta)|$ = 0.85) was much higher than that of the Blank group ($|\cos(\theta)|$ = 0.05), indicating a robust electrotactic response induced by EGD-generated EF. F-actin polarization is an important cytoskeleton feature related to cell directional migration [21]. Fluorescence staining showed that the EGD significantly promoted F-actin aggregation in the pre-migration segment of the cell population, while the distribution of F-actin in the Blank group was incoherent **(Figure 3F)**. This result further confirmed the exact role of EGD in cell electrotaxis induction.

Cell directional migration is a dynamic equilibrium process related to a variety of signal molecules. E-cadherin is a calcium ion-dependent cell adhesion glycoprotein mainly distributed in epithelial tissues, which mediates cell adhesion and connection [22]. As revealed by Western blotting, the expression of E-cadherin was significantly down-regulated in the EGD group, indicating that the electricity generated by TENGs could promote cell migration by inhibiting the expression of E-cadherin **(Figure 3I)**. PI3K/Akt is a classic pathway involved in cell migration and proliferation; PI3K promotes cell directional migration by activating electrotaxis in cells that respond to electrical signals [11]. As a downstream molecule of PI3K, the Akt can promote cell proliferation by reducing cyclin degradation when activated. EF also activates MAPK signaling through ERK 1/2 phosphorylation, thereby promoting cell proliferation and migration [23]. To evaluate whether EGD could activate electrical-related signaling to influence cell behavior, the phosphorylation status of key proteins in

PI3K/Akt and MAPK/ERK pathways were tested by Western blotting. It was shown that the levels of p-PI3K, p-Akt and the p-ERK1/2 were significantly upregulated in the EGD group, demonstrating that EF generated by EGD activated these pathways. Furthermore, we also inhibited the PI3K/Akt and MAPK/ERK pathways by blocking the phosphorylation of Akt and ERK using the PI3K inhibitor LY294002 and the ERK inhibitor U0126, respectively. Cell migration experiments demonstrated that blocking the phosphorylation of Akt and ERK resulted in a decrease in the directional migration ability of HaCaT cells in EDG-generated EF **(Figure S9, Supporting Information)**. Based on the above phenomena, it was confirmed that EGD could activate electrical-related signaling pathways such as PI3K/Akt and MAPK/ERK to regulate cell behavior.

Prolonged exposure to EGD-generated EF induced macrophage M2-like phenotype *in vitro*

In addition to epithelial migration, the activation of the immune system also plays an indispensable role in wound repair. Macrophages, as one of the most vital immune cells affecting wound healing, could transform into pro-inflammatory M1 or reparative M2 phenotypes to control inflammation or tissue repair, respectively [24]. M1 macrophages increase the secretion of IL-1β, TNF, and IL-18 and activate inducible iNOS to produce NO, thereby engulfing pathogens and intensifying the inflammatory processes. M2 macrophages, however, inhibit the inflammatory response by secreting IL-10 and arginase-1 (Arg-1), promoting positive wound repair and minimizing scar formation. During the healing process, the M2 transition in macrophages is essential for the resolution of inflammation and tipping the balance to tissue repair. By contrast, the defection of the M2 phenotype results in prolonged inflammation, chronic wound, and excessive scarring ultimately. EF stimulation is known to suppress the pro-inflammatory macrophage and the inflammatory response in a model of injured spinal cord in rat [25]. It is therefore curious for us to know whether a prolonged EF exposure would have an effect on the macrophage polarization *in vitro*, since the EGD-generated EF in our system showed excellent biosafety with the theoretical thermal energies one trillionth of that of the DC power. Interestingly, after 24 hours of intervention in the EGD group, macrophages presented with long spindle-shapes accompanied by prominent protrusions on the membrane, revealing a transition to the M2 phenotype from the perspective of morphology **(Figure 3J and Figure S10, Supporting Information)**. By using CD206, a commonly used marker for M2 macrophages, flow cytometry was applied to characterize the effect of EF on the phenotypes of macrophages. According to flow cytometry analysis, the EGD group showed an upregulated expression level of the M2-macrophage marker CD206 (89%), significantly higher than the Blank group (75.7%) **(Figure 3K, 3L and Figure S11, Supporting Information)**. These results for the first time

indicated that the EF produced by EGD could facilitate macrophage polarization toward the M2 phenotype, implying its potential in accelerating the transition from inflammatory to proliferative phase during the wound repair *in vivo*.

EGD effectively reshaped wound EF and accelerated wound repair with less scar formation in large full-thickness wounds in pigs

The *in vitro* tests confirmed the cellular regulation and immunomodulatory functions of the EF driven by TENGs. The effect of EGD treatment on large-scale full-thickness wounds *in vivo* was further assessed. Theoretically, EGD provides a combination treatment mode of integrated EF stimulation and NPWT to promote wound repair synergistically **(Figure 4A-4C)**: the periodically changing negative pressure in NPWT cleaned the wound against inflammation and provided a wound environment beneficial for tissue regeneration, e.g. the growth of granulation tissue [5]; TENGs driven by the periodically changing negative pressure in NPWT converted the mechanical energy into a compensating EF, facilitating the transition of reparative M2 macrophage and realizing the directional driven of epithelial cells. All the materials in the EGD exhibited high biocompatibility and were proven to be non-toxic according to a cytotoxicity test **(Figure S12, Supporting Information)**. The pig large full-thickness skin wound model (a diameter of 30 mm and depth of 5mm-sized circular defect) was established. The self-healing model was defined as the Blank group, and pigs treated with NPWT monotherapy were set as controls considering the effects of drainage and mechanical force on wound healing. To ensure that the EGD could provide effective and stable EF for wounds, the wound potentials and currents before and after EGD treatment were continuously monitored **(Figure S13, Supporting Information)**. According to the surgical photos and wound area analysis, the EGD promoted wound healing significantly **(Figure 4D-4G)**. In the early proliferative phase (Day 6), the proportion of the healed area in the EGD group was 53.48%, which was 1.93 and 7.35 times that of the NPWT monotherapy group (27.74%) and Blank group (7.28%) **(Figure 4E-4G)**. When the treatment was prolonged to 12 days, the majority of traumas in the EGD group were successfully repaired (90.37%), significantly higher than the healed area of the NPWT (72.52%) and Blank (55.21%) groups **(Figure 4E)**.

Healing of deep skin wounds induces hypertrophic scarring in human beings, which is a detrimental outcome for skin functionality [26]. The formation of scars not only affects aesthetics but also causes pain, itching, and dysfunction [27, 28]. There are many time-consuming and costly treatments, such as laser treatment, surgical treatment, microneedle treatment [29], pressure therapy [30], local drug injection [31], and the adoption of platelet-rich plasma [32], for the elimination of

abnormal scars. However, preventing scar formation in the early stages of wound healing remains a challenge. Accumulating evidence has directly linked wound inflammation and delayed healing with the extent of scar formation [33]. The design of the EGD system fully considered the prognosis of scar hyperplasia, and the reshaped EF could enable early intervention in scar formation by the induction of the reparative M2 macrophages and acceleration of wound healing. After 28 days of treatment, the EGD group showed the smallest scar area, which was only 51.90% of the scar area in the NPWT group and 29.58% in the Blank group **(Figure 4H, 4J and Figure S14, Supporting Information)**. The scar condition was further assessed by Vancouver Scar Scale (VSS), a gold standard for scar severity evaluation. The EGD group obtained the lowest VVS overall score (3 points), compared with the NPWT (8 points) and Blank groups (11 points) **(Figure 4I, Figure S11 and Table S1, Supporting Information)**. From the perspective of various indicators, the scar formation in the NPWT group was less than that in the Blank group, which might be due to the significant effects of negative pressure drainage and mechanical force on various cells important for wound healing, thereby reducing scar formation [34]; and the EGD treatment group was close to normal tissue in pigmentation, vascularity, and height. These results revealed the potential clinical benefit of EGD treatment on wound repair and scar suppression.

EGD expedited and reinforced the proliferation period of large full-thickness wound repair in pigs

The proliferative stage, as characterized by the formation of granulation tissue and re-epithelialization, is a crucial step for wound repair [2]. Granulation tissue, consisting of a large amount of blood vessels, provides the most basic support to re-epithelialization, since nutrients and oxygen are needed for epithelial migration and proliferation in the process of re-epithelialization [35, 36]. To understand the effect of the reshaped EF on the proliferative phase of wound repair, maturation of granulation tissue and re-epithelialization were examined by using H&E staining. As shown in **Figure 5A**, the EGD group had the most abundant neovascularization compared with NPWT and Blank groups **(Figure S15, Supporting Information)**. The pro-vascularization potential of EGD was attributed to the fact that the generated EF could promote the secretion of VEGF from vascular endothelial cells **(Figure S16, Supporting Information)**. Although NPWT promoted denser blood vessel distribution than the Blank group, its vascularization was not as prominent as that of the EGD group. This might be attributed to the induction of macrophage M2 phenotype by the compensatory EF in the EGD group, which facilitated an earlier transition from the inflammatory to the proliferative phase in those wounds. As shown by HE staining, the average densities of lymphocytes, neutrophils, and macrophages in the EGD group were much lower than those in the Blank group, and were also

significantly different from those in the NPWT group, confirming the inhibition of short- and long-term inflammation by EGD **(Figure S17, Supporting Information)**. The above results indicated that EGD had a better promoting effect on the regeneration of granulation tissue. Restoration of a complete epidermal barrier on the wound surface, known as re-epithelialization, is an essential feature of wound repair. Re-epithelialization could be assessed by the measurements of the length of the newly formed epidermis in wounds. After 6 days of treatment, the average length of the newly formed epidermis in the EGD group was 2724 μm, significantly longer than those in NPWT (686 μm) and Blank group (775 μm) **(Figure 5A, 5B)**. There was no significant difference in the thickness of the newly formed epidermis between these groups **(Figure 5A, 5C)**. The 12-day treatment also showed a similar trend of re-epithelialization **(Figure 5B, 5C)**. It is worth noting that although wound closure in the NPWT group was faster than that in the Blank group **(Figure 4D-4G)**, the length of the newly formed epidermis was similar between the two groups **(Figure 5A, 5B)**. This could be explained by the fact that NPWT facilitated wound closure by promoting contraction; however, it weakened endogenous EF and thus hindered re-epithelialization. Re-epithelialization suppression by weakened EF has been also observed in some chronic metabolic diseases, for example, the endogenous EF of the wounds in diabetics is only half that of normal patients, which severely affects the function of epithelial cells and eventually forms a chronic wound [10]. In our EGD system, the reshaped EF generated by TENGs compensated well for the weakening of the EF caused by NPWT, and the length of the newly formed epidermis at 12 days was 1.76 times and 1.80 times that of the NPWT and Blank groups, respectively. In addition, we established large animal models of third-degree burn wounds and infected wounds (ulcers) to demonstrate the broad applicability of EGD for the treatment of refractory wounds **(Figure S18-23, Supporting Information)**. EGD was shown to be beneficial in the treatment of burns and chronic wounds by recording changes in the wound area. HE staining indicated that EGD accelerated the recovery of burns and infected wounds by promoting wound re-epithelialization (consistent with acute wound healing mechanisms). The above results proved that EGD could cover a wide range of indications, and most acute and chronic wounds caused by different etiologies can be treated with EGD.

Wound re-epithelialization is determined by epithelial proliferation and migration; cell proliferation increases cell reserves for wound repair, and cell migration ensures that epithelial regeneration can be carried out efficiently and rapidly [37]. To more fully reveal the mechanisms of the reshaped EF on re-epithelialization, the proliferation and migration of epithelial cells were determined by immunohistochemical staining. Proliferating cell nuclear antigen (PCNA), a proliferating cell nuclear antigen and a cofactor of DNA polymerase, is a core marker for DNA

replication and cell proliferation [38]. Up-regulation of PCNA in the nucleus is consistent with active cell proliferation. From immunohistochemical staining, PCNA continued to be highly expressed in the EGD group on the 6th and 12th day of treatment **(Figure 5D, 5F)**; as a comparison, relatively low levels of PCNA were detected in the NPWT and Blank groups, confirming that the reshaped EF promoted the proliferation of epithelial cells *in vivo*. As mentioned above, E-cadherin, a cell surface glycoprotein, mediates intercellular adhesion mainly in epithelial tissues [22]. Down-regulation of E-cadherin weakens the adhesion between cells and then benefits cell migration. Expression of E-cadherin at the end of the newly formed epidermis in the EGD group was significantly lower than in the NPWT and Blank group **(Figure 5D, 5F)**, proving that the epithelial cells possessed a higher migration activity under the compensation EF. Taken together, these observations were consistent with the *in vitro* results, and confirmed that the reshaped EF could facilitate a transition from the inflammatory to the proliferative phase by inducing the M2 phenotypes of macrophages, and reinforce the proliferation period by promoting proliferation and migration of epithelial cells, finally accelerating wound re-epithelialization and achieving a rapid wound closure.

EGD advanced the remodeling period to enhance the quality of repaired tissue

As the final stage of wound repair, the remodeling phase begins at the end of re-epithelialization and lasts for several weeks or months to reconstruct the epithelial microstructure and the extracellular matrix in granulation tissue [39]. This phase determines if scarring will occur or the wound's strength will be compromised ultimately. However, since the barrier function of the skin has been restored during this process, there are few non-invasive treatments to intervene in the remodeling period. Continuous EF therapy positively affects the remodeling period without producing any new trauma. H&E staining at 28th day showed that the average thickness of the newly formed epidermis during the remodeling period in the EGD group was 183 μm **(Figure 6A)**, significantly thicker than the NPWT (90 μm) and Blank (45 μm) groups **(Figure 6B)**. Moreover, the cell stratification of the new epithelial tissue in the EGD group was close to the stratified squamous epithelium, that is, the histologic type of mature epithelial tissue. In addition, the appearance of rete pegs is another important sign of epithelial maturity, which tightly connects the newly formed epidermis and granulation tissue to avoid secondary exfoliation [40]. In the EGD group, a large number of rete peg structures could also be found in the center of the newly formed epidermis, the density of which was significantly higher than that of the NPWT and Blank groups **(Figure 6C)**. These observations confirmed that EGD significantly accelerated the maturation of epithelial tissue during the remodeling period.

In addition to the maturation of epithelium, the disorganized extracellular matrix in the granulation tissue is actively remodeled to form a new dermis during the remodeling phase, which ultimately forms scars [41]. Granulation tissue is largely comprised of collagen III that possesses relatively low stability and elastic tension due to its immature structure. During the remodeling phase, the type III collagen is partially replaced by the stronger collagen I to enhance the strength of repaired skin [42]. In normal adult skin, the ratio of type I collagen to type III collagen (I/III) is maintained at ~4:1 to ensure the strength and toughness of the skin. The Sirius red staining indicated that the contents of type I and III collagen in the Blank group were similar on the 28th day (I/III =1.03), while in the NPWT group the type I collagen increased with no decline in type III collagen. In contrast, a significant increase in type I collagen accompanied by a sharp decrease in type III collagen was observed in the EGD group **(Figure 6D, 6E).** The increased ratio of type I/III collagen indicated that the newly formed dermis in the EGD group was close to the normal skin dermis **(Figure S24, Supporting Information)**. In addition to the chemical composition, the order of the assembled structure of collagen also plays an important role in skin characteristics and scar formation. Compared with the random arrangement of collagen in the NPWT and Blank groups, the collagen in the EGD group were oriented along the reshaped EF and tightly arranged in a parallel manner **(Figure 6D, 6F)**, similar to normal skin tissue **(Figure S25, Supporting Information)**. These results showed that EGD effectively promoted the remodeling of the extracellular matrix and increased the quality of the repaired skin tissue, which accounted for the observed less scar formation macroscopically mentioned above **(Figure 4H-4J)**.

3. Conclusion

We have established a self-powered EGD therapy based on NPWT and TENG that can promote wound repair and reduce scars in a rapid and non-invasive manner **(Figure 6G)**. Detailed *in vitro* and *in vivo* experiments highlighted the advantages of EGD therapy over the current widely used clinical NPWT regimen in the treatment of large full-thickness skin wounds. As an “electrical adjuvant”, the cellular regulation and immunomodulatory functions of reshaped EF in EGD facilitated the inflammation/proliferation transition, accelerated the process of re-epithelialization in the proliferative period, and reconstructed the epithelial microstructure and the extracellular matrix in the remodeling stage. The EGD significantly promoted wound closure and improved the quality of repair, endowing the repaired skin tissue with a higher degree of maturity, stronger resistance to external forces, better avoidance of secondary damage, and less noticeable scars. A particularly

promising opportunity lies in diabetic dermatology where the EGD system could promote the repair of diabetic wounds by compensating for the pathological decrease of the endogenous EF. Other possibilities are those of clinical conditions using NPWT in the treatment of large or chronic wounds, performing an essential and synergistic effect in promoting healing. More importantly, the cost of upgrading NPWT to EGD therapy is only $6.78, allowing a wider range of patients to obtain a better prognosis with the less financial burden **(Table S2, Supporting Information)**. The development of EGD will provide new ideas for the progress of self-powered electrical stimulation combined therapy equipment and devices.

4. Experimental Section

Fabrication of TENG built into the EGD

The working mode of produced TENG is the classical vertical contact-separation mode. The size of TENG was 2 mm*2.5 cm * 5 cm. The two triboelectric layers were the thin aluminum (Al) sheet and PTFE film, which were sanded 3-4 times with sandpaper [43]. The first unit of TENG was Cu / PET / PTFE. The PET sheet prevented the collapse of the first unit. And the Cu electrode was connected to the ground and had a polarization voltage of 5 kV. The second unit of TENG is Al. Al is both an electrode and a triboelectric layer. Then TENG was packaged by PI film.

Preparation of the EGD

The EGD was mainly composed of TENG, polyurethane (PU) foam dressings, rectifier bridges, wires, and electrodes. The PU foam dressing was purchased from 3M company (the website for purchase: https://www.3m.com/3M/en_US/p/d/b5005265140/) with a size of 15 *10 *3 cm^3, and a pore size of ~600 μm. Two wires of TENG were connected to the two input ends of the rectifier, and two wires of electrodes were connected to the output end of the rectifier. The rectifier bridge is packaged by PI film. The electrodes were fabricated by using ultra-aspect ratio Ag nanowires with a diameter of 70 nm and a length of 100-200 μm as the conductive component, and porous PU foam was used as a flexible polymer matrix to support the conductive network **(Figure 1B)** [44]. The purpose made foam dressing was cut into a ring with an inner diameter of 4 cm and an outer diameter of 5 cm, and connected with the positive output end of the rectifier bridge. A rod-like purpose made foam dressing was inserted with a length of 1 cm and a diameter of 1 mm into the polyurethane foam dressing in the middle of the ring-shaped foam dressing, and connected the rod-like dressing electrode with the wire at the negative output end of the rectifier bridge. The EGD was sealed in a closed environment by a medical sterile dressing.

NCD function setting

The structure of the NCD mainly included a liquid storage pot, a vacuum pump, an inflator pump, and a control module. The liquid storage pot was connected to a vacuum pump, which stored the drainage liquid. The inflator pump was used to pump gas into the EGD, and the vacuum pump pumped out the gas from the EGD. The control module was used to control the working time of the vacuum pump and inflator pump, which caused the deformation of the dressing.

Characterization methods

The scanning electron microscopy (SEM) image was collected with a Hitachi field emission scanning electron microscope (SU 8020). The electrometer (Keithley 6517B) and oscilloscope (Teledyne LeCroy HD 4096) were used to measure the voltage and current. The negative pressure was monitored by an electronic barometer (AZ82152).

Electrolyte analysis of exudates

Immerse PU foam dressing (1 day) soaked with wound exudate in PBS for 3 days. The leaching solution was collected and placed in a serum electrolyte analyzer to detect the concentrations of K^+, Na^+, Ca^{2+}, and Cl^-.

Cell culture

HaCaT cells were used for cell migration experiments. HaCaT cells are immortalized epidermal cells with similar functions and characteristics to normal epidermal cells, which are easier to obtain and culture than normal epidermal cells. However, the migration direction under directional EF is completely opposite to that of normal epidermal cells (HaCaT cells migrate to the positive electrode, while normal tissue epidermal cells migrate to the negative electrode). The HaCaT cells and THP-1 cells were obtained from the Cell Bank of the Chinese Academy of Sciences in Beijing, China. HaCaT cells were cultured in 1640 medium (SH30809.01B, Hyclone) containing 10% fetal bovine serum (FBS, Gibco) and 1% penicillin/streptomycin (GA3502, Genview). THP-1 cells were cultured in 1640 medium (SH30809.01B, Hyclone) containing 10% fetal bovine serum (FBS, Gibco), 0.05 mM β-mercaptoethanol (M8210, Solarbio), and 1% penicillin/streptomycin (GA3502, Genview). The cell culture condition is a humid incubator (CCL-170B-8, ESCO) with 5% CO_2 at 37°C.

Whether placing two rod electrodes on opposite sides of a petri dish or using the outer-annular/center-punctiform electrodes, both types of electrode arrangements produce directional EFs, which are equivalent to some extent. According to the COMSOL simulation, the side views of the directional EF generated by the two electrode arrangements described above are almost identical **(Figure S26, Supporting Information)**. The selection of electrodes is mainly based on experimental requirements. In the cell experiments, we chose two rod electrodes (positive and negative,

respectively) to apply a directional EF to the cells. Because for the outer-annular/center-punctiform electrodes, it is difficult to obtain the migration trajectories of cells in a uniform EF under the microscope (top-down perspective). In contrast, rod electrodes have a larger area of homogeneous EF under the microscope view, which is more suitable for observing cell localization.

Safety assessment

The HaCaT cells were stimulated by EF through a carbon electrode for 48 h. The Cell Viability/Cytotoxicity Detection and CCK-8 were used to assess cell viability of the HaCaT cells in the Blank group (no EF), DC group (5 V), and EGD group. The confocal fluorescence microscope (Leica SP8) was employed to capture images. The microplate reader (BioRad iMark) was used to test absorbance.

Imaging of motility

The HaCaT cells were stimulated by EF through carbon electrodes. The time-lapse imaging was performed using a Zeiss imaging system (Carl Zeiss Meditec, Jena) and the images were recorded every 5 minutes for 3 hours.

Quantitative analysis of cell migration

The position of the nucleus was tracked every 5 minutes and quantified the motility of the cells by software (Image–Pro Plus 6.0). The cosθ was used to evaluate the directionality of cells, which represented the angle between the field vector and the direction of cell migration. The trajectory velocity (Tt/t) and displacement speed (Td/t) were used to quantify the cell migration velocity.

Immunofluorescence of HaCaT cells

After EF stimulation, the cells were fixed with 4% paraformaldehyde for 30 minutes at 25□. After rinsing with PBS three times, samples were blocked in 5% goat serum in PBS for 1 h at 37□. Phalloidin (1:200 dilution, incubated 2 h) and DAPI (1:100 dilution, incubated 10 min) were respectively used to stain the cytoskeleton and cell nucleus. The confocal fluorescence microscope (Leica SP8) was employed to capture images.

Western blots analysis

The HaCaT cells were suspended in the lysis buffer for 30 min, the lysates were sonicated for 4 seconds and separated by centrifugation at 14,000 r for 15 min at 4°C, then the supernatants were subsequently collected. Protein concentrations were determined using the BCA protein assay kit (Sigma). A total of 20 μg of protein were separated by the 6~12% gradient SDS-PAGE and transferred onto polyvinylidene difluoride (PVDF) membranes. After being blocked by 5% non-fat milk for 3h, the blots were incubated overnight at 4°C with the primary antibody, and washed thoroughly with PBS three times at 10min, then incubated with corresponding secondary antibodies at room temperature

for 1 h. Then after being washed thoroughly with PBS three times and the bands were detected with ECL KIT. The primary antibodies were as follows: anti-E-cadherin (1:1000, CST), anti Erk1/2 (1:1000, CST), anti p-Erk1/2 (1:1000, CST), anti PI3K (1:1000), CST anti p-PI3K (1:1000, CST), anti Akt (1:1000, CST), anti p-Akt (1:1000, CST), anti β-actin (1:5000, Proteintech), the second antibodies were at 1:4000 dilution. The images were quantified with the Quantity One 4.1 software (Bio-Rad, USA).

Blocking of signaling pathways

The HaCaT cells were pretreated with LY294002 (PI3K inhibitor; Sigma, 50 mM) or with U0126 (ERK1/2 inhibitor; Sigma, 50 mM) for 1 h to block Akt and ERK, respectively. Blocker-treated HaCaT cells were cultured in EGD-generated EFs for 3 hours. Simultaneously with electric field stimulation, real-time imaging was performed using a Zeiss imaging system (Carl Zeiss Meditec, Jena), and the Image–Pro Plus 6.0 were recorded every 5 minutes for 3 hours. The position of the nucleus was tracked every 5 minutes and quantified the motility of the cells by software (Image–Pro Plus 6.0).

ELISA test

The EF generated by EGD was applied to HUVECs *in vitro*. Then we collected cell culture medium at 0 h, 3 h, and 6 h, and detected VEGF content in culture fluids by ELISA kits.

Polarization of macrophages

THP-1 cells were cultured in 12-well plates at a density of $2*10^6$ cells with 75 ng/ mL PMA (P6741, Solarbio) and complete medium for 3 days. Macrophages from the Blank group and EF group were cultured in the medium with 10 ng/ mL IL-4(P00021, Solarbio) for 24 h. The microscope (Lecia DMI6000B) is used to observe the morphology of cells.

Flow cytometry

The macrophages were scraped off and collected in phosphate buffered saline (PBS, P1033, Solarbio). Then, flow cytometry was used to evaluate the expression of CD11b and CD206 of the cell suspension. CD11b was quantified by incubating with 1.25 μL FIRC anti-mouse/human CD11b (Biolegend) for 30 minutes. CD206 was quantified by incubating with 1.25 μL APC anti-human CD206 (MMR) (Biolegend) for 20 minutes. FITC Rat IgG2b /κ isotype Ctrl (Biolegend) and APC Mouse IgG1/ κ isotype Ctrl (Biolegend) were set as homotypic controls. All these determinations were performed in the cell quantitative analyzer (ACCURI C6) and analyzed using FlowJo software.

Animal culture and grouping

The experiments were performed on 12 female Bama miniature pigs (8-12 weeks old, 20–25 kg body weight) without any skin diseases. Pigs were kept in the animal center of the Third Military Medical University without pathogens at 25□. General anesthesia and analgesia procedures were administered according to the Bama Pig Guide Provided by the University Animal Resources

Committee. All experimental procedures were reviewed and approved by the University Committee on Animal Resources.

Animal experiment

The 40 cm * 40 cm size of back hairs were removed by using a scalpel and depilatory cream. In an acute wound model, three full-thickness skin wounds with a diameter of 3 cm (including the partial subcutaneous adipose tissue), two of which were parallel to and 5 cm away from the midline and one of which was on the middle line with the same 10 cm away from the other wounds were excised on the back. In the burn wound model, three third-degree burn wounds were formed by pressing the scalding device at 200°C on normal skin for 30 seconds under certain pressure [45]. The wound location and size were consistent with the acute wound model. In order to comply with clinical norms and experimental ethics, burn wounds needed to be debridement within 24 hours before subsequent experiments (third-degree burn wounds are contraindications of NPWT, and can only be treated after debridement). In the infected wound model, three full-thickness skin wounds were created following the acute wound protocol. Wounds were infected with *Staphylococcus aureus* (200 μL PBS) at a concentration of 10^9 CFU/mL for 1 day (recorded as -1 day). Colonized bacteria and necrotic tissue were subsequently removed from the wound surface for subsequent experiments.

The three wounds on each pig were randomly assigned to three groups. The wounds in the Blank group were covered with only the polyurethane foam dressings. The NPWT group treated the wound by negative pressure and dressings. In the EGD group, wounds were treated with a combination of EF and negative pressure. On the 6^{th} day, the PU foam dressing on the wound surface was changed in each group, which was in line with the dressing change cycle (3-7 d) for clinical NPWT treatment. On the 6^{th}, 12^{th} , and 28^{th} day, the wound status in the acute wound model was observed and recorded and wound tissues were collected for observation and analysis. The wound status in the burn and infected wound model was recorded on the 0^{th}, 12^{th} and 18^{th} day. The surface areas of the wounds were measured. Remaining wound area (%) = [wound area／initial wound area] × 100.

Wound electrical measurement

The electrometer (Keithley 6517B) and oscilloscope (Teledyne LeCroy HD 4096) were used to measure the wound potential and current. **Figure S27 (Supporting Information)** is a schematics diagram illustrating the method for measuring wound potential and current. The potential difference obtained by separating the positive and negative electrodes of the electrometer by 1 mm was the average EF intensity of the area. Between the wound and the normal skin, we uniformly selected 81 samples to measure their average EF intensity, and imported the coordinate information into origin 9.0 to draw a 3D colormap surface type map. The endogenous potential difference of the wound was

measured by placing the positive electrode of the electrometer on normal skin at the wound edge and the negative electrode at the wound center. When EGD was used for wound treatment, the positive electrode of the built-in TENG was placed at the edge of the wound, and the negative electrode was placed at the center of the wound. The reshaping wound potential in the EGD group was measured by connecting an electrometer in parallel to the wound (the positive electrode at the edge of the wound and the negative electrode at the center of the wound). Fig. 2G showed the current passing through the entire wound surface, that is, the wound was applied as a load. The endogenous current of the wound was measured by placing the positive electrode of the electrometer at the wound edge and the negative electrode at the center of the wound. Notably, when testing the current produced by EGD applied to the wound, we measured the reshaped wound current by connecting an electrometer in series with the built-in TENG and the wound.

Histology

The tissues were soaked in 4% paraformaldehyde overnight, then dehydrated with graded series of ethanol and embedded in paraffin blocks for sectioning at 4 μm. Tissue sections were Processed with hematoxylin and eosin (H&E) staining, immunohistochemical (IHC) staining, and Sirius red staining to analyze. In the IHC, the sections were blocked with 5% goat serum in PBS for 1 h at room temperature and then incubated with anti-PCNA (1:200, CST) and anti-E-cadherin (Abcam, 1:1000) overnight, then after washing three times with PBS, secondary antibodies were added for 1 h (dilution 1: 100), finally, the staining was visualized after incubation with a DAB-H_2O_2 solution for 5 min and counterstained with hematoxylin. After observation under a microscope, the positive expression rate was analyzed by Image–Pro Plus 6.0.

Statistical analysis

The statistical significance of the differences was determined by one-way ANOVA. All cell experiments were repeated three times. In animal experiments, the wound analysis and statistics of each group were obtained from three independent wounds of three pigs. Statistics of HE staining, Gram staining, immunohistochemical staining, and Sirius red staining of wound tissue in all groups were derived from the results of parallel experiments on three pigs. Data were analyzed as mean ± standard error of mean (S.E.M.) in GraphPad Prism v. 6. Image–Pro Plus 6.0, Origin 2018 and GraphPad Prism v. 6 were used for data plotting. * $p < 0.05$, ** $p < 0.01$ and *** $p < 0.001$ were considered statistically significant.

Supporting Information

Supporting Information is available from the Wiley Online Library or from the author.

Acknowledgements

Ruizeng Luo, Yi Liang, Jinrui Yang, contributed equally to this paper. We are grateful to all the laboratory members for their cooperation in this study. The authors thank Prof. Jianda Dong of Ningxia Medical University for his help in the analysis of H&E staining. The authors are grateful for the support received from the Strategic Priority Research Program of Chinese Academy of Sciences (XDA16021101), the National Natural Science Foundations of China (Nos. T2125003, 81873936, 61875015, 51902344 and 81971770), the Clinical Technology Innovation and Cultivation Project of Army Medical University (CX2019JS102), Beijing Natural Science Foundation (JQ20038 and L212010), the National Key Research and Development Program of China (2021YFB3201200, 2022YFB3200192), the Chongqing Natural Science Foundation (cstc2019jscxmsxmX0101) and the outstanding project of the Youth training Program of Military Medical Science and Technology (21QNPY026).

References

[1] P. Martin, *Science* **1997**, *276*, 75-81.

[2] M. K. Strecker-McGraw, T. R. Jones, D. G. Baer, *Emerg. Med. Clin. North Am.* **2007**, *25*, 1-22.

[3] Y. Long, H. Wei, J. Li, G. Yao, B. Yu, D. Ni, A. LF Gibson, X. Lan, Y. Jiang, W. Cai, X. Wang, *ACS Nano* **2018**, *12*, 12533-12540.

[4] S. Dhivya, V. V. Padma, E. Santhini, *Biomedicine* **2015**, *5*, 24-28.

[5] M. Khamaisi, S. Balanson, *Diabetes Metab. Res. Rev.* **2017**, *33*, e2929.

[6] Z. Iheozor-Ejiofor, K. Newton, J. C. Dumville, M. L. Costa, G. Norman, J. Bruce, *Cochrane Database Syst. Rev.* **2018***, 7*, CD012522.

[7] C. D. McCaig, A. M. Rajnicek, B. Song, M. Zhao, *Physiol. Rev.* **2005**, *85*, 943-978.

[8] C. Martin-Granados, C. D. McCaig, **2014**, *3*, 127-138.

[9] R. Luo, J. Dai, J. Zhang, Z. Li, *Adv. Healthc. Mater.* **2021,** *10*, 2100557.

[10] B. Reid, M. Zhao, *Adv. Wound Car*e (New Rochelle) **2014**, *3*, 184-201.

[11] M. Zhao, B. Song, J. Pu, T. Wada, B. Reid, G. Tai, F. Wang, A. Guo, P. Walczysko, Y. Gu, T. Sasaki, A. Suzuki, J. V. Forrester, H. R. Bourne, P. N. Devreotes, C. D. McCaig, J. M. Penninger, *Nature* **2006,** *442*, 457-460.

[12] K. Y. Nishimura, R. R. Isseroff, R. Nuccitelli, *J. Cell Sci.* **1996**, *109*, 199-207.

[13] S. Wang, L. Lin, Z. L. Wang, *Nano Lett.* **2012**, *12*, 6339-6346.

[14] G. Zhu, C. Pan, W. Guo, C. Y. Chen, Y. Zhou, R. Yu, Z. L. Wang, *Nano Lett.* **2012**, *12*, 4960-4965.

[15] H. Ouyang, Z. Liu, N. Li, B. Shi, Y. Zou, F. Xie, Y. Ma, Z. Li, H. Li, Q. Zheng, X. Qu, Y. Fan, Z. L. Wang, H. Zhang, Z. Li, *Nat. Commun.* **2019**, *10*, 1821.

[16] L. Lin, Y. Xie, S. Wang, W. Wu, S. Niu, X. Wen, Z. L. Wang, *ACS Nano* **2013**, *7*, 8266-8274.

[17] G. Zhu, Z. H. Lin, Q. Jing, P. Bai, C. Pan, Y. Yang, Y. Zhou, Z. L.Wang, *Nano Lett.* **2013**, *13*, 847-853.

[18] Z. L. Wang, *ACS Nano* **2013**, *7*, 9533-9557.

[19] C. Wade, S. E. Wolf, R. Salinas, J. A. Jones, R. Rivera, L. Hourigan, T. Baskin, J. Linfoot, E. A. Mann, K. Chung, M. Dubick, *Nutr. Clin. Pract.* **2010**, *25*, 510-516.

[20] L. C. Kloth, *Adv. Wound Care (New Rochelle)* **2014**, *3*, 81-90.

[21] C. Huang, K. Jacobson, M. D. Schaller, *J. Cell. Sci.* **2004**, *117*, 4619-4628.

[22] W. J. Guo, F. G. Giancotti, *Nat. Rev. Mol. Cell Biol.* **2004,** *5*, 816-826.

[23] E. Konstantinou, Z. Zagoriti, A. Pyriochou, K. Poulas, *Cells* **2020**, *9*, 1924.

[24] R. Orihuela, C. A. McPherson, G. J. Harry, *Br. J. Pharmacol.* **2016,** *173*, 649-665.

[25] X. L. Huo, G. H. Zhang, C. Z. Wu, C. Zhang, *39th Annual International Conference of the IEEE-Engineering-in-Medicine-and-Biology-Society (EMBC))* **2017**, 1958-1961.

[26] J. Simkin, T. R. Gawriluk, J. C. Gensel, A. W. Seifert, *Elife* **2017**, *6*, e24623.

[27] O. Bock, G. Schmid-Ott, P. Malewski, U. Mrowietz, *Arch. Dermatol. Res.* **2006,** *297*, 433-438.

[28] D. A. Potter, D. Veitch, G. A. Johnston, *Br. J. Hosp. Med.* **2019**, *80*, C166-C171.

[29] I. B. S. Sitohang, S. A. P. Sirait, J. Suryanegara, *Int. Wound J.*, **2021,** *18*, 577-585.

[30] P. C. Esselman, B. D. Thombs, G. Magyar-Russell, J. A. Fauerbach, *Am. J. Phys. Med. Rehabil.* **2006,** *85*, 383-413.

[31] W. Manuskiatti, R. E. Fitzpatrick, *Arch. Dermatol.* **2002,** *138*, 1149-1155.

[32] S. Min, J. Y. Yoon, S. Y. Park, J. Moon, H. H. Kwon, D. H. Suh, *Lasers Surg. Med.* **2018**, *50,* 302-310.

[33] X. Xu, S. Gu, X. Huang, J. Ren, Y. Gu, C. Wei, X. Lian, H. Li, Y. Gao, R. Jin, B. Gu, T. Zan, Z. Wang, *Burns Trauma* **2020**, *8*, tkaa006.

[34] G. C. Gurtner, S. Werner, Y. Barrandon, M. T. Longaker, *Nature* **2008***, 453*, 314-321.

[35] D. Hoffman, M. Koch, T. Krieg, S. A. Eming, *Wound Repair Regen.* **2007**, *15*, A138-A138.

[36] V. Falanga, *Lancet* **2005**, *366*, 1736-1743.

[37] Y. Liang, H. Tian, J. Liu, Y. Lv, Y. Wang, J. Zhang, Y. Huang, *Bioelectrochemistry* **2020**, *135*, 107578.

[38] G. L. Moldovan, B. Pfander, S. Jentsch, *Cell* **2007**, *129*, 665-679 (2007).

[39] J. Q. Coentro, E. Pugliese, G. Hanley, M. Raghunath, D. I. Zeugolis, *Adv. Drug Del. Rev.* **2019**, *146*, 37-59.

[40] G. Sa, *J. Dent. Res.* **2017**, *96*, 1546-1554.

[41] H. N. Lovvorn, D. T. Cheung, M. E. Nimni, N. Perelman, J. M. Estes, N. S. Adzick, *J. Pediatr. Surg.* **1999**, *34*, 218-223.

[42] T. Hurme, H. Kalimo, M. Sandberg, M. Lehto, E. Vuorio, *Lab. Invest.* **1991**, *64*, 76-84.

[43] L. Zhao, Q. Zheng, H. Ouyang, H. Li, L. Yan, B. Shi, Z. Li, *Nano Energy* **2016**, *28*, 172-178.

[44] Y. Chen, Y. Liang, J. Liu, J. Yang, N. Jia, C. Zhu, J. Zhang, *Biomater. Sci.* **2021**, *9*, 238-251.

[45] Y. I. Shen, H. G. Song, A. Papa, J. Burke, S. W. Volk, S. Gerecht, *J. Invest. Dermatol.* **2015***, 135*, 2519-2529.

Figures

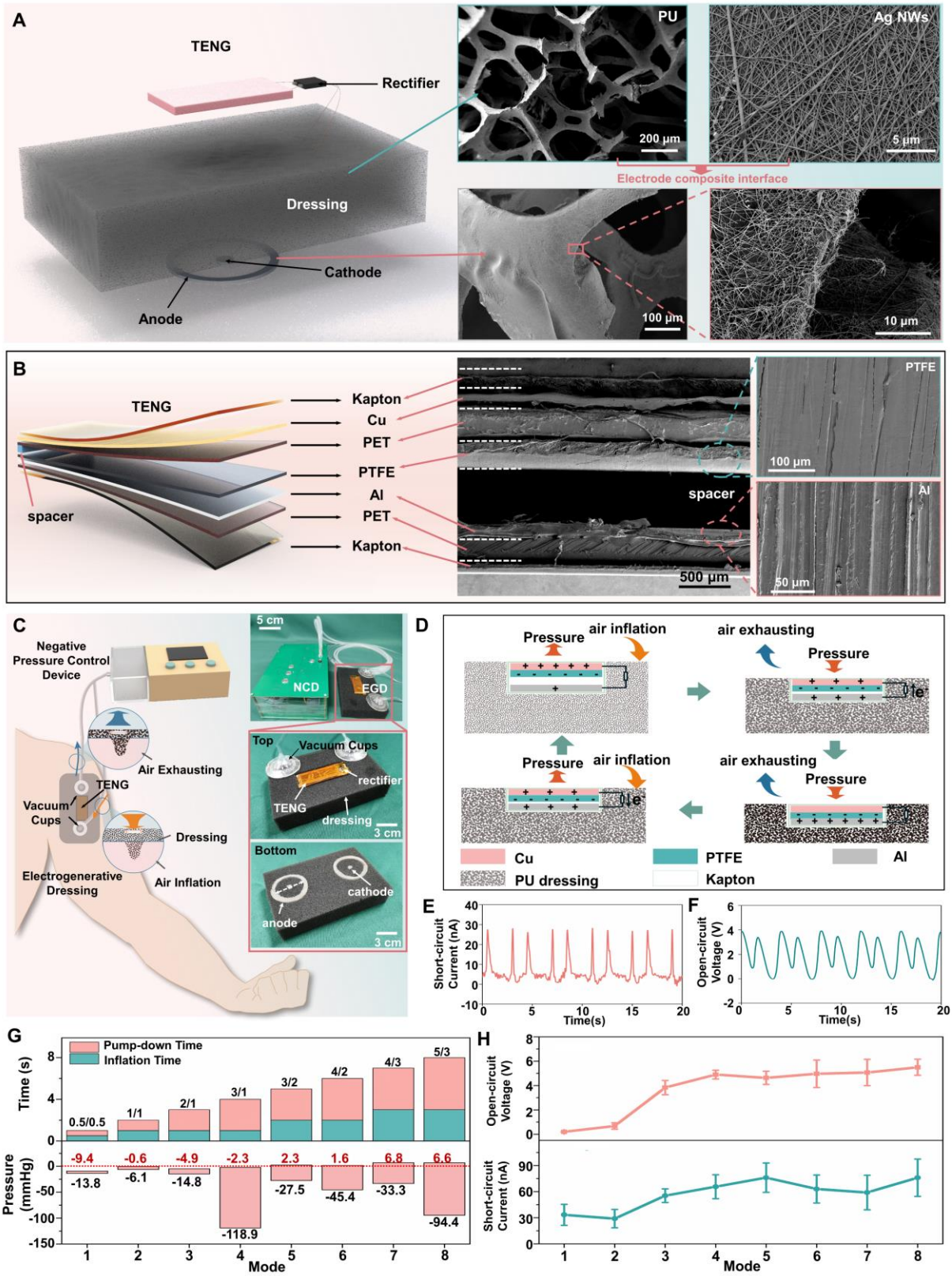

Figure 1. Structure and working principle of the EGD-NCD system. (A) Exploded-view schematic and

structure of the EGD. The right pictures are the SEM images of PU dressing and electrodes (PU dressing compounded with Ag NWs). A porous dressing is a prerequisite for stable changes of negative pressure. (B) Structure and materials of built-in TENG. The right pictures are the cross-section of the TENG and the surface morphology of the friction layers (PTFE and Al) under SEM. (C) Overview of the EGD-NCD system. The EGD-NCD system changes the negative pressure and combined with a TENG to generate directional electric fields to the wound. Top: a dressing that consists of a TENG and rectifier. Bottom: an annular anode and the punctiform cathode. (D) Power generation principle of EGD. (E, F) Open-circuit voltage (E) and short-circuit current (F) of EGD after full-wave rectification in the 4th mode (0.25 Hz). (G) Working time, negative pressure of EGD in different working modes. The red numbers are the low values of the negative pressure in the EGD, and the black numbers are the high values of the negative pressure. (H) Voltage and current of EGD in different working modes (n=3 independent samples. Data are presented as mean ± S.E.M.).

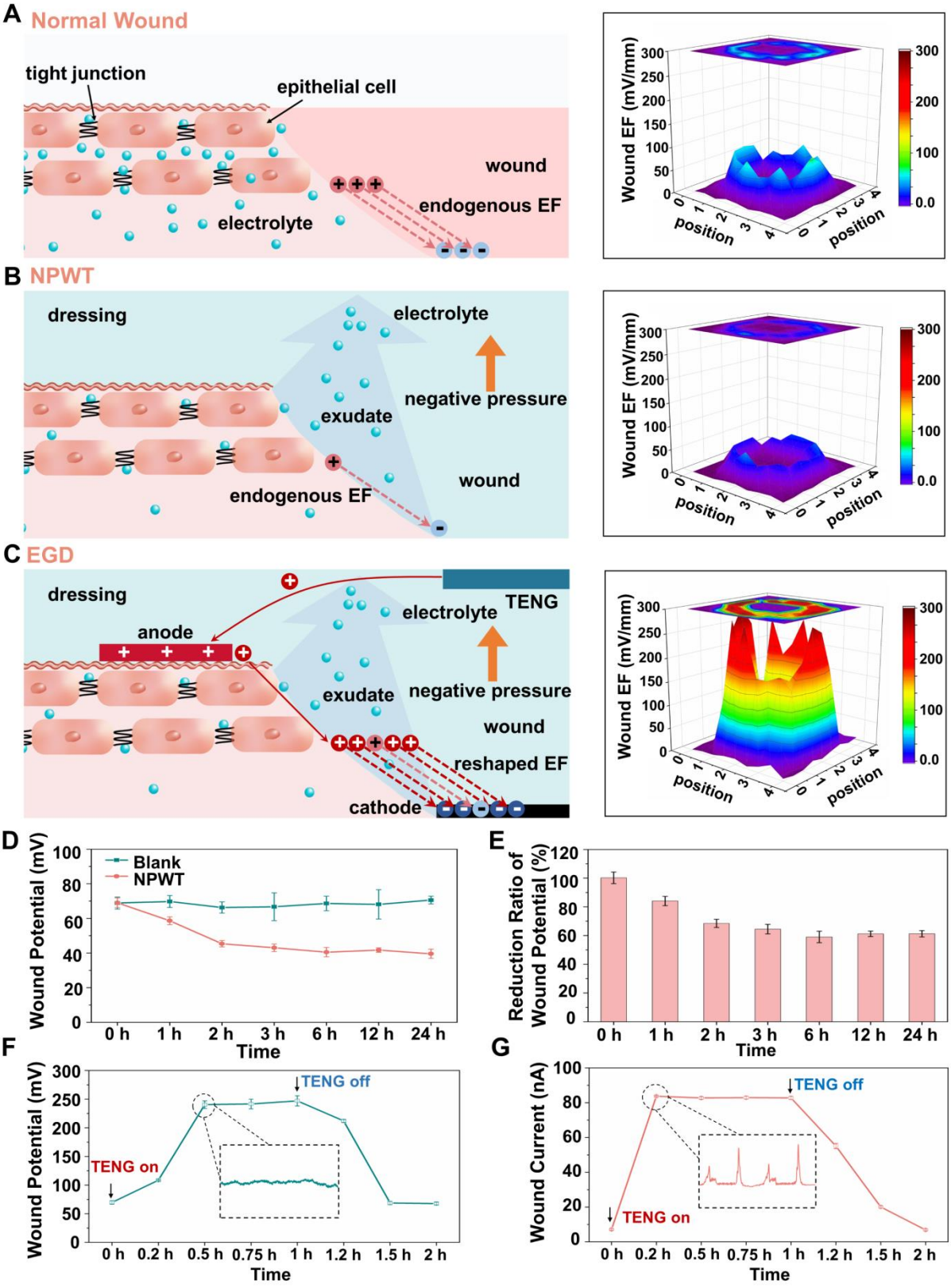

Figure 2. Effect of the NPWT and EGD on wound potential. (A-C) Illustration and three-dimensional profile of the wound potential in Blank control group (A), NPWT group (B), and EGD group (C). The

insets show the wound potential is asymmetric. (D) Wound potential weakened by the continuous NPWT. (E) The ratio of wound potential in the NPWT group compared with the Blank group. (F) Effect of the EGD on wound potential. The wound potential is increased by EGD and maintained at a stable level after 30 min of the EGD treatment. After EGD removal, the wound potential is returned to the initial value gradually. The dashed black box is the waveform of the instantaneous wound potential. (G) Effect of the EGD on wound current. The dashed black box is the waveform of the instantaneous wound current. n=3 independent samples. Data are presented as mean ± S.E.M.

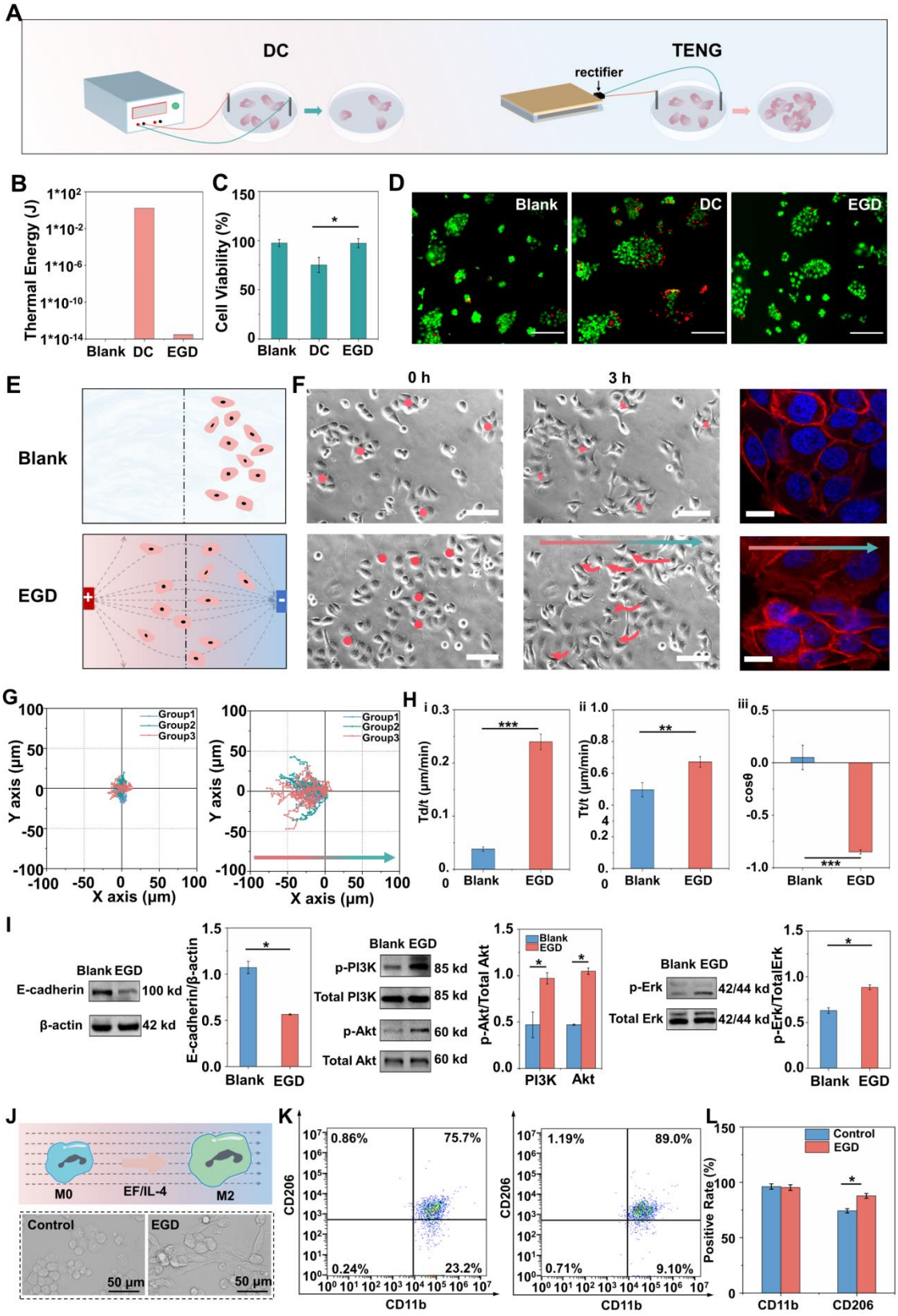

Figure 3. Features of HaCaT cells by EGD *in vitro*. (A) Illustration of the electric field applied to the HaCaT cells. (B) The thermal energy of DC supply power (5 V) and the EGD (the 4th mode). The

thermal energy of DC is much greater than that of the EGD with the same voltage intensity. (C) Effect of different EFs on cell viability of HaCaT cells. (D) Live/Dead Cell Staining of HaCaT cells in the Blank, DC, and EGD groups. The red cells are dead cells and the green fluorescence shows that the cells are alive. The white bar is 200 μm. (E) Illustration of HaCaT cell migration under the directional EF. (F) Migration of HaCaT cells in the Blank group and the EGD group. Cellular morphology with F-actin fluorescence staining in groups shows the distribution of cytoskeleton during the HaCaT cell migration. The left bar is 100 μm, and the bar of F-actin fluorescence staining is 20 μm. (G) Migration trajectory of HaCaT cells in the Blank group (3 h) and the EGD group (3 h). (H) Analysis of cell migration. The statistical graphs show the displacement speed (i), trajectory speed (ii), and directedness (cosθ) (iii) of HaCaT cells. (n=30 independent samples. ** $p < 0.01$and *** $p < 0.001$. All statistical analyses were performed by one-way ANOVA. Data are presented as mean ± S.E.M.) (I) Expression of E-cadherin, p-PI3K, p-Akt, and p-Erk1/2 protein through the western blotting at the 4th mode. (J) Illustration of macrophage polarization from M0 to M2 and photograph of macrophage shape. (K) Expression of cellular markers in the control group and EGD group. (L) Positive rate of cell markers in the control and EGD groups. CD11b is the marker of macrophage, and CD206 is the marker of M2 macrophage. n=3 independent samples in Figure 3I, 3L. * $p < 0.05$, ** $p < 0.01$and *** $p < 0.001$. All statistical analyses were performed by one-way ANOVA. Data are presented as mean ± S.E.M.

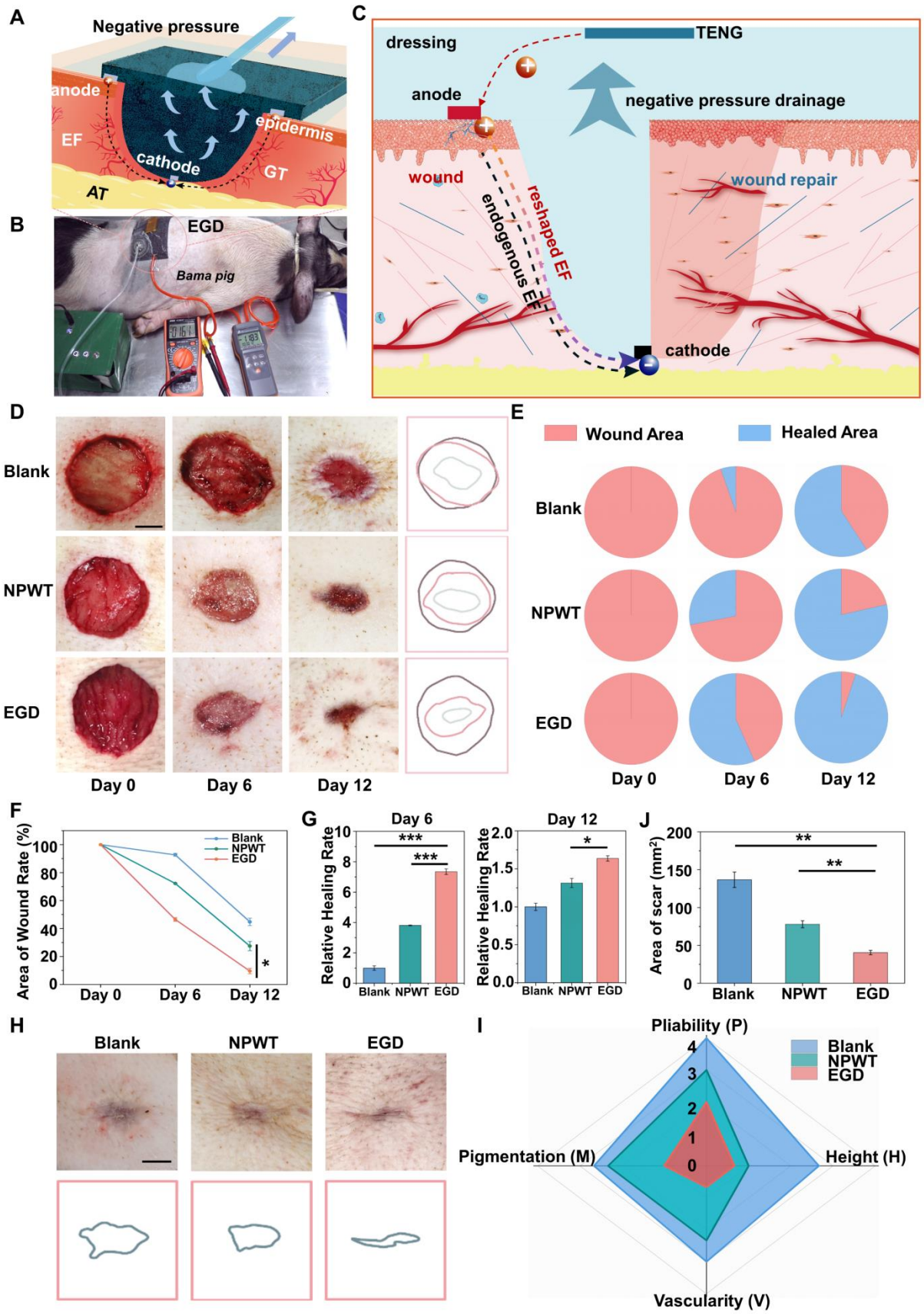

Figure 4. Therapeutic efficacies of the EGD on wound repair. (A) Multiple effects of the EGD on wounds, including negative pressure and electrical field. (B) Photograph of the EGD-NCD system in pig. (C) Effects of the EGD-NCD system on wound repair. (D) Photographs of the wound and wound contour under different treatment modes, the blank bar is 1 cm. (E) Comparison of the healed area with the unhealed area in groups. (F) Area of wound rate. (G) The relative healing rate of wounds in the NPWT and EGD groups compared with the Blank group. The left graph is the relative healing rate of wounds within 6 days, and the right graph is the relative healing rate of wounds within 12 days. (H) Photographs of scar and scar contour under different treatments (28 days), the blank bar is 1 cm. (I) Vancouver scar score of the repaired tissue. (J) Area of the scar. n=4 independent samples in Figure 4F, 4G, 4J. * $p < 0.05$, ** $p < 0.01$and *** $p < 0.001$. All statistical analyses were performed by one-way ANOVA. Data are presented as mean ± S.E.M.

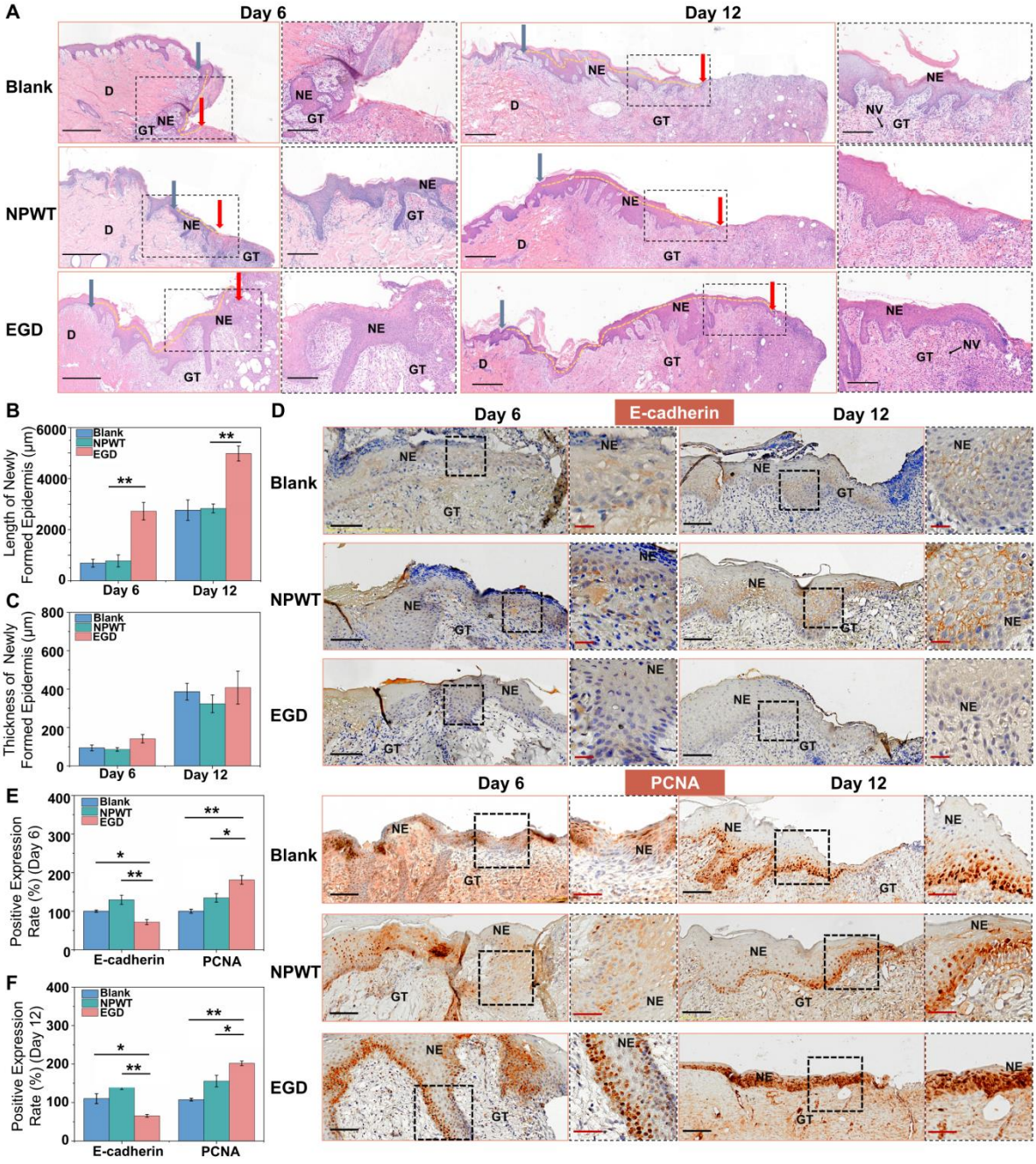

Figure 5. Assessments of wound healing among different treatments on histopathology. (A) H&E staining of wound tissue (day 6 and day 12). The blue arrow indicates the wound edge, and the red arrow indicates the end of the newly formed epidermis; the dashed black box is enlarged to the right (the left bar is 500 μm and the right bar is 200 μm). D, dermis; GT, granulation tissue; NE, new epithelium; NV, new vessels. (B) Length of the newly formed epidermis in different groups. (C) The thickness of newly formed epidermis in different groups. (n=9 independent samples. All statistical analyses were performed by one-way ANOVA. Data are presented as mean ± S.E.M.) (D) Immunohistochemical staining of E-cadherin and PCNA in different groups. GT, granulation tissue;

NE, the new epithelium (the black bar is 100 μm, the red bar in the E-cadherin group is 25 μm, the red bar in the PCNA group is 50 μm. and E-cadherin and PCNA are orange particles). (E, F) Quantitative analysis of PCNA and E-cadherin positive staining on the 6^{th} (E) and 12^{th} day (F). n=3 independent samples in Figure 5B, 5E, 5F. n=9 independent samples in Figure 5C. * $p < 0.05$ and ** $p < 0.01$. All statistical analyses were performed by one-way ANOVA. Data are presented as mean ± S.E.M.

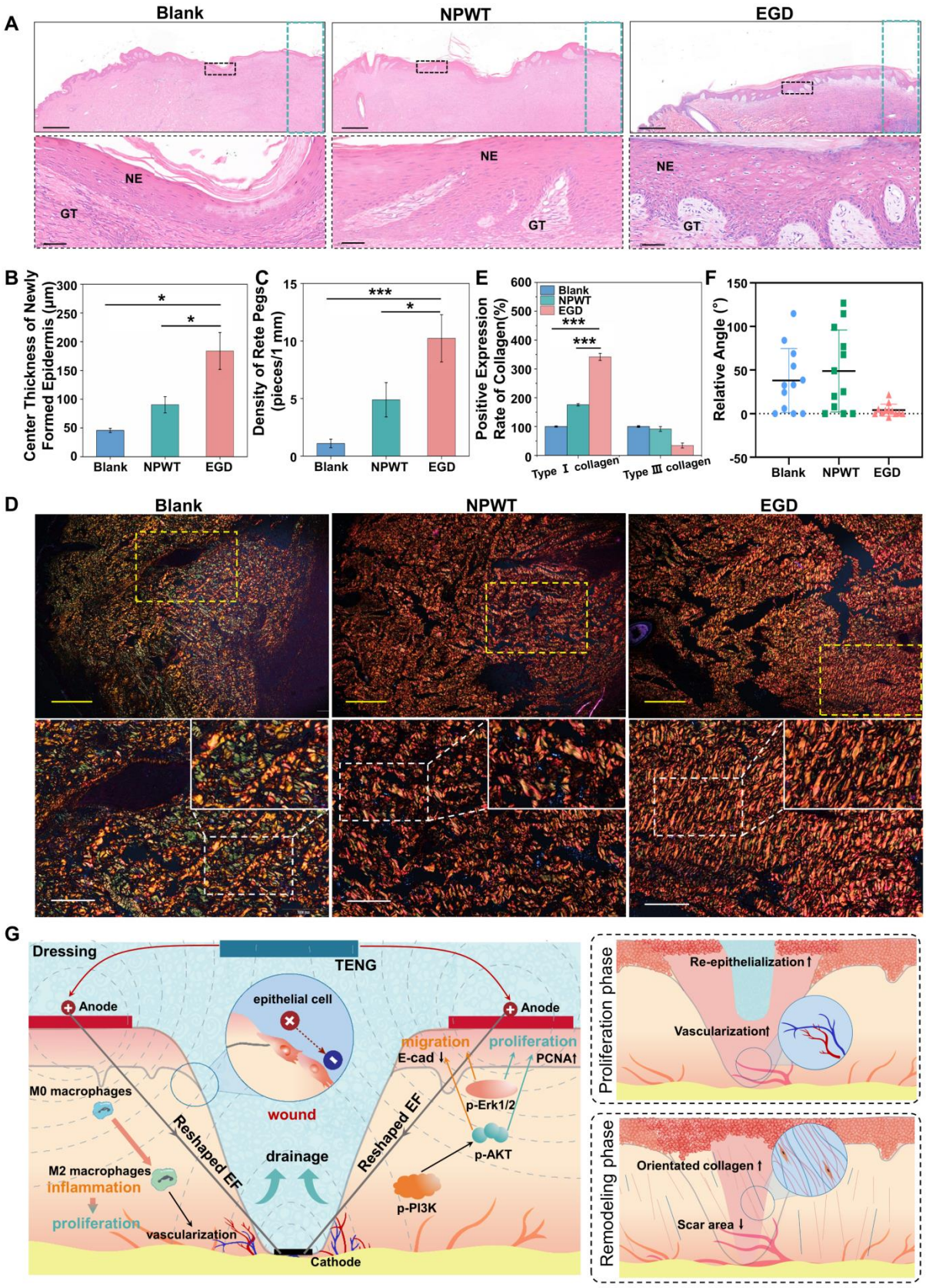

Figure 6. EGD advanced remodeling period. (A) H&E staining of wounds in the Blank group, NPWT group, and EGD group (28 days). The black small dashed box is the enlarged image on below, the

green large dashed box is the center of the newly formed epidermis (the upper bar is 500 μm and the lower bar is 50 μm). GT, granulation tissue; NE, new epithelium. (B) The thickness of re-epithelialized center in groups. (C) The density of rete pegs in H&E staining confirms the maturation of the epithelial tissue in groups. (D) Sirius red staining in the center of the repaired tissue in different groups (28 days). Green fluorescence is type III collagen, and red fluorescence is type I collagen. The yellow dashed box is the enlarged image on the below (the yellow upper bar is 500 μm and the white lower bar is 200 μm). (E) The relative content of collagen compared with the Blank group. (n=12 independent samples in Figure 6B, 6C, 6E. All statistical analyses were performed by one-way ANOVA. Data are presented as mean ± S.E.M.) (F) Relative angle of collagen in different groups. (G) Mechanisms of promoting wound healing by the typical EGD system. The EGD accelerates the polarization of macrophages to M2 macrophages, strengthens cell proliferation and migration, augments angiogenesis and re-epithelialization, enhances the orientation of collagen, and decreases the scars. n=3 independent samples in Figure 6B, 6C, 6E. * $p < 0.05$ and *** $p < 0.001$. All statistical analyses were performed by one-way ANOVA. Data are presented as mean ± S.E.M.

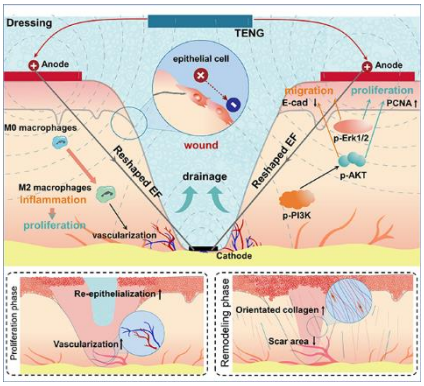

The non-invasive electrogenerative dressing (EGD) is designed by integrating triboelectric nanogenerators (TENG) with negative pressure wound therapy (NPWT), which makes a great breakthrough in wound repair and scar prevention with clinical transformation potential. The EGD accelerates the polarization of macrophages to M2 macrophages, strengthens cell proliferation and migration, augments angiogenesis and re-epithelialization, enhances orientation of collagen, and reduces scars.